OPTICAL PROPERTIES OF SAHARAN AND ASIAN DUST:

APPLICATION TO RADIATIVE TRANSFER SIMULATIONS

A Thesis

by

GUANGYANG FANG

Submitted to the Office of Graduate Studies of
Texas A&M University
in partial fulfillment of the requirements for the degree of

MASTER OF SCIENCE

May 2012

Major Subject: Atmospheric Sciences

OPTICAL PROPERTIES OF SAHARAN AND ASIAN DUST:

APPLICATION TO RADIATIVE TRANSFER SIMULATIONS

A Thesis

by

GUANGYANG FANG

Submitted to the Office of Graduate Studies of
Texas A&M University
in partial fulfillment of the requirements for the degree of

MASTER OF SCIENCE

Approved by:

Chair of Committee,	Ping Yang
Committee Members,	Sarah D. Brooks
	Kai Chang
Head of Department,	Kenneth Bowman

May 2012

Major Subject: Atmospheric Sciences

ABSTRACT

Optical Properties of Saharan Dust and Asian Dust:

Application to Radiative Transfer Simulations. (May 2012)

Guangyang Fang, B.S., Nanjing University of Information Science & Technology;

M.S., Chinese Academy of Sciences

Chair of Advisory Committee: Dr. Ping Yang

Because the bulk optical properties of dust are largely dependent on their chemical composition, published reports from numerous dust field studies enabled us to compile observation data sets to derive the effective complex refractive indices of Saharan and Asian dust. We considered the individual mineral components as aggregates and used the Bruggeman approximation to derive the effective refractive indices. Using the results, we calculated the single-scattering properties, including phase matrix, single-scattering albedo and asymmetry factor, with a combination of the T-matrix method and an improved geometric optics method (IGOM). The single-scattering properties were averaged by the measured particle size distribution to provide bulk optical properties for radiative transfer simulations. Using a Rapid Radiative Transfer Model (RRTM), the radiative forcing of mineral dust was computed at both the top of the atmosphere and the surface.

By analyzing samples from various in-situ measurements, we assumed the Saharan and Asian dust to have average volume compositions and average aspect ratios. The effective refractive indices for Saharan and Asian dust were derived based on the assumed composition models. Bulk optical properties were integrated using the modified log-normal particle size distributions. The aspect ratio assumed in this study is 1.6 for both Saharan and Asian dust. The longwave radiative (IR) forcings at the top of the atmosphere (TOA) and at the surface were found to be positive and sensitive to wavelength. The shortwave (solar) radiative forcing at TOA, was also positive, but may possibly have been due to the strong absorption components considered in the composition models.

ACKNOWLEDGEMENTS

I would like to thank my advisor and committee chair, Dr. Ping Yang, for supporting my research and education in Texas A&M University. I also thank my committee members, Dr. Sarah D. Brooks, and Dr. Kai Chang, for their guidance and support throughout the course of this research.

Thanks also go to the faculty and staff in the Atmospheric Sciences Department. I want to extend my gratitude to all the excellent members in my research group for providing generous help during my two years' study at Texas A&M University

Finally, thanks to my family and good friends in China for their forever love and help.

TABLE OF CONTENTS

Page

LIST OF FIGURES

LIST OF TABLES

1. INTRODUCTION: THE IMPORTANCE OF THE RESEARCH

Mineral dust aerosols are very important constituents of the atmosphere and primarily influence the climate system by scattering and absorbing radiation. The Intergovernmental Panel on Climate Change (IPCC 2007) report illustrates the direct aerosol radiative effect to be approximately $-0.5 \pm 0.4 W/m^2$. Although anthropogenic aerosols play an important role in climate change, the majorities of aerosols are natural ones and can impact cloud properties, convective cloud dynamics, and the development of tropical storms (Jones et al. 2004). The optical properties of mineral dust aerosols are critical to radiative transfer and remote sensing simulations. However, dust properties are affected by many factors including geographic locations, dust sources and chemical and physical transformations occurring during transport within the atmosphere. The bulk optical properties of dust are largely dependent on their chemical components and volume fraction, and a reliable set of spectral refractive indices is desirable. Therefore, by compiling observation data sets from various published literature, we will attempt to derive the effective complex refractive indices of Saharan and Asian dusts, which originate from two of the major sources of atmospheric aerosols.

Remote sensing with the help of passive and active satellites has provided global and long temporal observations of dust aerosols. The widely used passive satellite instruments include: Advanced Very High Resolution Radiometer (AVHRR) (Carlson 1979; Husar et al. 1997), Totoal Ozone Mapping Spectrometer (TOMS) (Prospero et al.

This thesis follows the style of *Journal of the Atmospheric Sciences*.

2002), Ozone Monitoring Instrument (OMI) (Torres et al. 2007), and the Moderate Resolution Imaging Spectroradiometer (MODIS) (Kaufman et al. 2005). However, most of them are unable to detect the desert regions with a high surface reflectance and thus cannot distinguish between the bright surface and the dust aerosols. To solve this problem, a “Deep Blue” algorithm introduced by Hsu et al. (2004) was applied to MODIS and SeaWIFS (Sea-viewing Wide Field-of-view Sensor) data to calculate the optical depth over deserts based on the fact that the blue part of the visible spectrum of desert surfaces has a much lower reflectance (Hus et al. 2004). The infrared spectrum has also been used by the SEVIRI (Spinning Enhanced Visible and Infrared Imager) on the Meteoscat-8 to detect dust aerosols over deserts (Schmetz et al. 2002), making it possible to detect at nighttime. The Could-Aerosol Lidar and Infrared Pathfinder Satellite Observation (CALIPSO) carrying the Cloud-Aerosol Lidar with Orthogonal Polarization (CALIOP) is able to distinguish dust from other aerosol types by using the depolarization ratio (Hu et al. 2007), but little work has been done in this area. The Aerosol Robotic Network (AERONET) is a worldwide ground-based sunphotometers network which can measure the aerosol optical depth at visible and near infrared wavelengths; however, the observation sites are limited, especially over broad desert regions.

Even though satellite remote sensing has contributed to the study of mineral aerosols in recent years, the in-situ observations such as aircraft observations cannot be replaced. Some important dust aerosol field campaigns in the Saharan and Asian regions include: the Saharan Dust Experiment (SHADE) flight in 2002 (Haywood et al. 2003);

Saharan Mineral Dust Experiment field campaign (SUMUM) in 2003 (Kandler et al. 2007; Otto et al. 2009); Dust and Biomass Burning Experiment (DABEX) in 2008 (Osborne et al. 2008); Dust Outflow and Deposition to the Ocean (DODO) in-situ flight in 2006 (McConnell et al. 2008); ACE-Asian (Huebert et al. 2003) and TRACEP-P (Jacob et al. 2003). These in-situ observations of mineral dust have provided a large amount of information for our study. By comparing in-situ observed data with satellite retrievals, we can validate the satellite observations.

We have considered the individual mineral components as aggregates and have applied the Bruggeman approximation to calculate the effective refractive indices. Using the derived spectral complex refractive indices and considering the mineral dust as randomly oriented spheroidal particles, we have calculated a database of the optical properties including phase matrix, extinction efficiency, single-scattering albedo, and asymmetry factor (g factor). Furthermore, radiative forcing at both the top and bottom of the atmosphere was calculated.

2. METHODOLOGY AND BACKGROUND

2.1 Effective medium approximations

Two sets of quantities are often used to describe the optical properties of materials: the complex refractive index, $m = m_r + im_i$, and the complex dielectric function (relative permittivity), $\varepsilon = \varepsilon_r + i\varepsilon_i$ (Bohren and Huffman 1983). These two optical quantities are dependent and have the following relationships:

$$\varepsilon = m^2 = (m_r + m_i)^2 = (m_r^2 - m_i^2) + 2im_r m_i \tag{2.1}$$

$$\varepsilon_r = m_r^2 - m_i^2 \tag{2.2}$$

$$\varepsilon_r = 2m_r m_i \tag{2.3}$$

$$m_r = \sqrt{\frac{\sqrt{\varepsilon_r^2 + \varepsilon_i^2} + \varepsilon_r}{2}} \tag{2.4}$$

$$m_i = \sqrt{\frac{\sqrt{\varepsilon_r^2 + \varepsilon_i^2} - \varepsilon_r}{2}} \tag{2.5}$$

where m_r and m_i are nonnegative.

Either of these two quantities may be preferable in different situations. For instance, when considering wave propagation, the complex refractive index is preferred. However, when considering the microscopic mechanisms responsible for optical effects, it is preferable to use the complex dielectric function (relative permittivity) (Bohren and Huffman 1983). That is why the permittivity (ε) is used in expressions of the effective

medium approximations. In our study, we considered the mineral dust particles to be inhomogeneous, thus, it was more convenient to use ε.

Many effective medium approximations are used in optics, each with its own merits and shortcomings. The Maxwell Garnett theory and the Bruggeman theory are the most widely used medium approximations and are derived from the same integral equation, but under different sets of approximations (Bohren and Huffman 1983). The volume average approximation is also often used (Sokolik and Toon 1999).

The Maxwell Garnett approximation assumes that solid inclusions are embedded in a homogeneous matrix and that the volume fraction (f_i) of the inclusions must be relatively small (f_i <<1%). Under these assumptions, the following formula holds

$$\frac{\varepsilon_{eff} - \varepsilon_m}{\varepsilon_{eff} + 2\varepsilon_m} = f_i \frac{\varepsilon_i - \varepsilon_m}{\varepsilon_i + 2\varepsilon_m} \tag{2.6}$$

where ε_{eff} is the effective permittivity, ε_m is the matrix permittivity, and ε_i is the inclusion permittivity. ε_{eff} can be expressed as:

$$\varepsilon_{eff} = \varepsilon_m \left[1 + \frac{3 f_i (\frac{\varepsilon_i - \varepsilon_m}{\varepsilon_i + 2\varepsilon_m})}{1 - f_i (\frac{\varepsilon_i - \varepsilon_m}{\varepsilon_i + 2\varepsilon_m})} \right] \tag{2.7}$$

and was first derived by Maxwell Garnett (1904).

Bruggeman (1935) derived the expression for the two-phase system

$$f_a \frac{\varepsilon_a - \varepsilon_{eff}}{\varepsilon_a + 2\varepsilon_{eff}} + f_b \frac{\varepsilon_b - \varepsilon_{eff}}{\varepsilon_b + 2\varepsilon_{eff}} = 0 \tag{2.8}$$

where f_a and f_b are the volume fractions of the two constituents, and ε_a and ε_b are the permittivities.

The Bruggeman approximation does not distinguish which component is the inclusion and which component is the matrix, and both components are treated symmetrically, which makes the Bruggeman effective medium approximation suitable for a completely random inhomogeneous medium. Therefore, we chose the Bruggeman approximation in order to avoid distinguishing inclusions and matrices from other components, and because more than two components in a medium system can be effectively treated. The multi-component system equation is

$$\sum_i f_i \frac{\varepsilon_i - \varepsilon_{eff}}{\varepsilon_i + 2\varepsilon_{eff}} = 0 \tag{2.9}$$

where *i* is an arbitrary number of components and the sum is the total number. Note that the volume fraction of all the components should be unity, i.e., $\sum_i f_i = 1$.

2.2 Light scattering theory

The light scattering field is extensive and its study is often limited to the scattering of single particles in the framework of classical electromagnetic theory and linear optics (Bohren and Huffman 1983). We only consider the single scattering of particles.

The Maxwell equations govern classical electrodynamics, and assuming SI units, have the form

$$\nabla \cdot \vec{D} = \rho \tag{2.10}$$

$$\nabla \cdot \vec{B} = 0 \tag{2.11}$$

$$\nabla \times \vec{E} = -\frac{\partial \vec{B}}{\partial t} \tag{2.12}$$

$$\nabla \times \vec{H} = \vec{J} + \frac{\partial \vec{D}}{\partial t} \tag{2.13}$$

where $\vec{D}$ is the electric displacement, $\vec{E}$ is the electric field, $\vec{B}$ is the magnetic induction, $\vec{H}$ is the magnetic field, ρ is the density of electric charge, and $\vec{J}$ is the electric current vector.

Considering a macroscopic and homogeneous medium, we have

$$\vec{D} = \varepsilon_0 (1 + \chi)\vec{E} \tag{2.14}$$

$$\vec{B} = \mu \vec{H} \tag{2.15}$$

$$\vec{J} = \sigma \vec{E} \tag{2.16}$$

where ε_0 is the permittivity of free space, χ is the electric susceptibility of the medium, μ is the magnetic permeability of the medium, and σ is the conductivity.

With the previous assumptions, Maxwell's equations are reduced to a set of two equations:

$$\varepsilon_0 (1 + \chi) \frac{\partial \vec{E}}{\partial t} = \nabla \times \vec{H} - \sigma \vec{E} \tag{2.17}$$

$$\mu \frac{\partial \vec{H}}{\partial t} = -\nabla \times \vec{E} \tag{2.18}$$

with only two field variables, $\vec{E}$ and $\vec{H}$, and can be solved in a time domain.

In our study, randomly oriented symmetric scattering particles are considered. The single-scattering of light can be described by the extinction cross section, σ_{ext}, scattering cross section, σ_{sca}, and the dimensionless Stokes scattering matrix in the following. They are also the single-scattering optical properties we will compute in Section 4.

$$F(\theta)=\begin{bmatrix} a_1(\theta) & b_1(\theta) & 0 & 0 \\ b_1(\theta) & a_2(\theta) & 0 & 0 \\ 0 & 0 & a_3(\theta) & b_2(\theta) \\ 0 & 0 & -b_2(\theta) & a_4(\theta) \end{bmatrix} \tag{2.19}$$

where θ is the scattering angle, and the $a_1(\theta)$ is the phase function satisfying the following normalization

$$\frac{1}{2}\int_0^{\pi} a_1(\theta)\sin(\theta)d\theta = 1 \tag{2.20}$$

The asymmetry parameter of the phase function is defined as

$$g=\langle\cos\theta\rangle=\frac{1}{2}\int_{-1}^{1} d(\cos\theta)a_1(\theta)\cos\theta \tag{2.21}$$

In all cases the following relations hold

$$\sigma_{ext}=\sigma_{sca}+\sigma_{abs} \tag{2.22}$$

The probability that a photon incident on a small element survives is called the single-scattering albedo

$$\omega=\frac{\sigma_{sca}}{\sigma_{ext}} \tag{2.23}$$

The Stokes vector is defined as a column with Stokes parameters *I, Q, U,* and *V*.

$$I = \begin{bmatrix} I \\ Q \\ U \\ V \end{bmatrix} \tag{2.24}$$

where parameter I is the intensity, and Q, U, V represent the polarization of the light. The Stokes parameters are real numbers and have the following relation with fully polarized radiation

$$I^2 = Q^2 + U^2 + V^2 \tag{2.25}$$

3. REFRACTIVE INDICES OF SAHARAN DUST AND ASIAN DUST

The effective refractive indices of Saharan dust and Asian dust were derived. Two effective medium approximations based on the Kramers-Kronig (K-K) relations, the Maxwell Garnett (MG) approximation and the Bruggeman approximation can be used to derive the optical constants such as the complex refractive index in the nanostructure system (Lucarini et al. 2005). Volume mixing is another approximation which can give results close to the Bruggeman approximation, and the results are in good agreement with the measurements of the complex refractive indices (Sokolik and Toon 1999).

3.1 Mineralogical composition models

In order to calculate the complex indices of refraction of Saharan dust and Asian dust, we need different samples from the regions and the volume fractions of each component. Many past in-situ experiments listed in Table 1 provide abundant data sources for our study. By averaging the volume fractions of all mineral components from the various measurements we can obtain the bulk mineralogical composition. However, not all the optical constants for each compound are available and we have assumed mineral dust models, see Figures 1 and 2.

Figure 1 shows the volume fractions for Saharan dust. The main components are illite (47%) and quartz (20%). Sulfate (2%) is a large proportion of the mixture when the particle size is small. Although iron oxide (1%) is present only a small proportion, it is a major contributor to the absorption of the particles. It has been proven that the effective medium refractive index is very sensitive to the proportion of iron oxides such as hematite and goethite (McConnell et al. 2008) but we have ignored the optical constants for goethite as they are rare. Figure 2 shows the volume fractions for Asian dust. Quartz at 45% and clay at 35% dominate the composition and to emphasize the importance of soot, we have assumed as much as 8% in volume. However, from the optical properties computation and radiative transfer simulations, it appears that the large amount of soot is not realistic, but due to soot's strong absorption, the importance of this component cannot be ignored.

TABLE 1. The chemical and mineralogical composition data sources.

Experiments	Time	Reference
Sahara		
SHADE (Saharan Dust Experiment) flight	2002	Haywood et al. 2003
SAMUM (Saharan Mineral Dust Experiment) Field campaign	2003	Kandler et al. 2007; Otto et al. 2009; Petzold et al. 2008
DABEX (Dust and Biomass Burning Experiment	2008	Osborne et al. 2008
DODO (Dust Outflow and Deposition to the Ocean) In-situ flight in (Senegal) Mauritania	2006	McConnell et al. 2008
Asia		
ACE-Asia	2003	Huebert et al. 2003
TRACEP-P	2003	Jacob et al. 2003

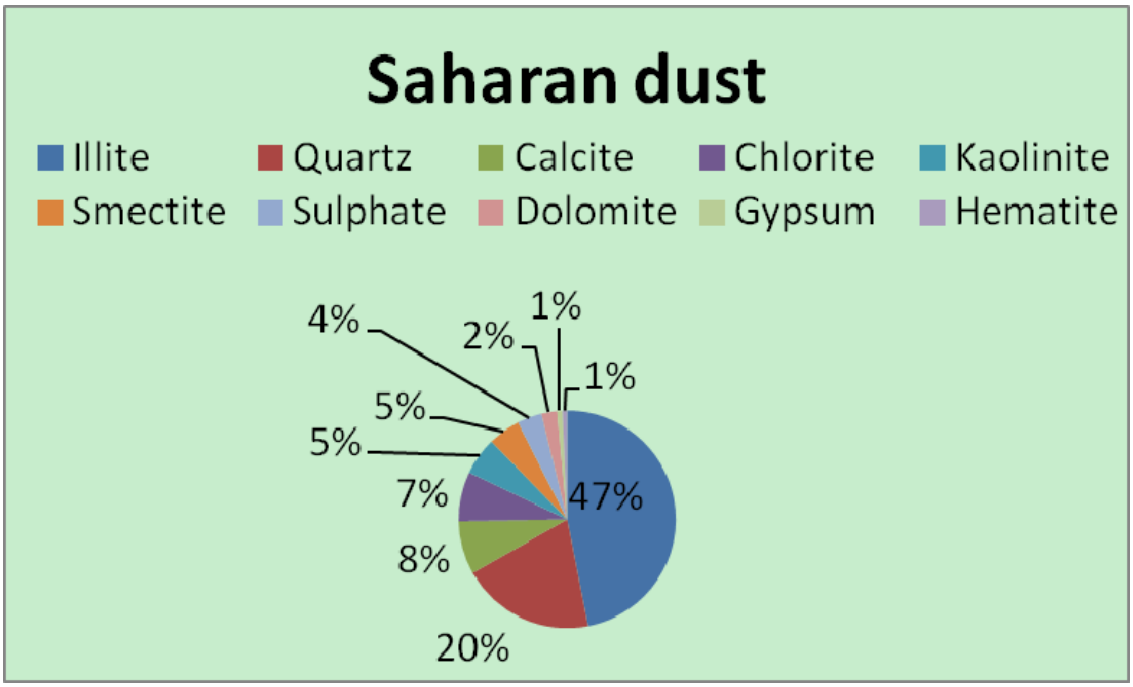

FIG. 1. Volume fraction of different components of Saharan dust

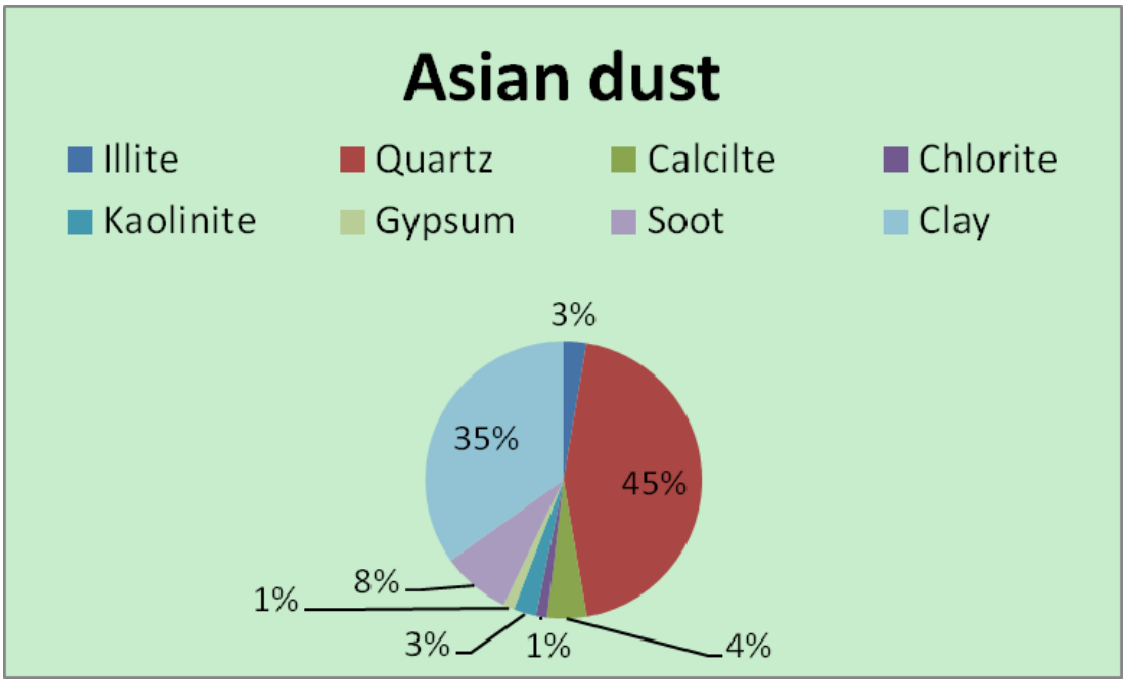

FIG. 2. Volume fraction of different components of Asian dust

3.2 Refractive indices of different components

The refractive indices of different components we considered in the composition models are needed for the Bruggeman approximation. The values were drawn from various literature reports, which are shown in Table 2. The wavelength ranges differ from individual to individual, and we have resorted to more than one report to obtain a complete set of spectral refractive indices from UV to thermal IR (0.02-50 μm). The data has been complied by hand to insure its accuracy. Some of the constituents were not used in this study, but the sources are listed in the table for future reference.

Figures 3 and 4 show the real and imaginary parts of the compiled refractive indices for some of the major components listed in Table 2. The values oscillate a great deal with the wavelength. The real part of the refractive index of quartz is as high as 8 and the imaginary part is as high as 7. Hematite is strongly absorptive and has the highest real refractive index at 11 and an imaginary refractive index of 10. Soot also has a large imaginary refractive index and its strong absorption is stable throughout the spectrum.

TABLE 2. References for the complex refractive indices of major constituents of mineral dust.

Constituents	Wavelength (μm)	Reference
Quartz	7.14-50.0	Popova et al. 1972
Amorphous form	7.14-25.0	Steyer et al. 1974
Crystalline form	0.736-36.0	Peterson and Weinman. 1969
	0.04-1000	Ivlev and Popova. 1972
	2-25	Philipp 1985
Silicates	0.185-2.6	Egan and Hilgeman 1979
Kaolinite	5-25	Roush et al. 1991
	2.5-200	Querry 1987
	0.13-2.5	Arakawa et al. 1997
	5-100	Glotch et al. 2007
Illite	0.185-2.6	Egan and Hilgeman 1979
	2.5-200	Querry 1987
	5-100	Glotch et al. 2007
Chlorite	2.5-50	Mooney and Knacke 1985
Serpentine	2.5-50	Mooney and Knacke 1985
	5-25	Roush et al. 1991
	5-100	Glotch et al. 2007
Feldspar	0.185-2.6	Egan and Hilgeman 1979
Mica	0.185-2.6	Egan and Hilgeman 1979

TABLE 2. Continued.

Constituents	Wavelength (μm)	Reference
Montmorillonite	0.185-2.6	Egan and Hilgeman 1979
	5.0-40	Toon et al. 1977
	2.5-200	Querry 1987
	0.2-2.5	Arakawa et al. 1997
Carbonate	2-32.8	Querry et al. 1978
Calcite	2.5-333.33	Long et al. 1993
Amorphous	0.2-6	Ivlev and Popova 1972
Crystalline	2-20	Tropf 1998
Sulfates	2.5-25	Palmer and William 1975
Ammonium	2.5-40	Volz 1973
sulphate	0.3-40	Toon et al 1976
mascagnite	2-20	Shettle and Fenn 1979
Gypsum	2.5-333.33	Long et al 1993
	0.2-6	Ivlev and Popova 1972
Iron-rich Wustite	0.5-200	Henning et al 1995
Goethite	0.45-0.75	Beddi and Cervelle 1993
Magnetite	0.25-0.7	Gillespie and Lindberg 1992
	0.21-55.556	Querry 1985

TABLE 2. Continued.

Constituents	Wavelength (μm)	Reference
Hematite	0.2-50	Querry et al. 1978
	0.21-55.56	Querry 1985
	8.3-50.0	Popova et al. 1972
	0.45-0.75	Bedidi and Cervelle 1993
	0.35-0.65	Shettle and Fenn 1979
	6.25-50	Gillespie and Lindberg 1992
	5-100	Marra et al. 2005
Soot	0.2-40	Shettle and Fenn 1979
	0.2-40	WCRP 1986
	0.5-0.75	Batten 1984
	0.26-55.556	Querry 1987
Sodium Chloride	0.2-100	Toon et al. 1976
	0.22-166.667	Querry 1987
Corundum	0.2-333	Toon et al. 1976
Sapphire	0.2-6	Ivlev and Popova 1972
	0.2-55.556	Querry 1985
Nitrate	2.17-20	Jarzembski et al. 2003
Clay (mont, kaoli and illite)	2.5-200	Querry 1987
Dolomite	2.5-50	Querry 1987

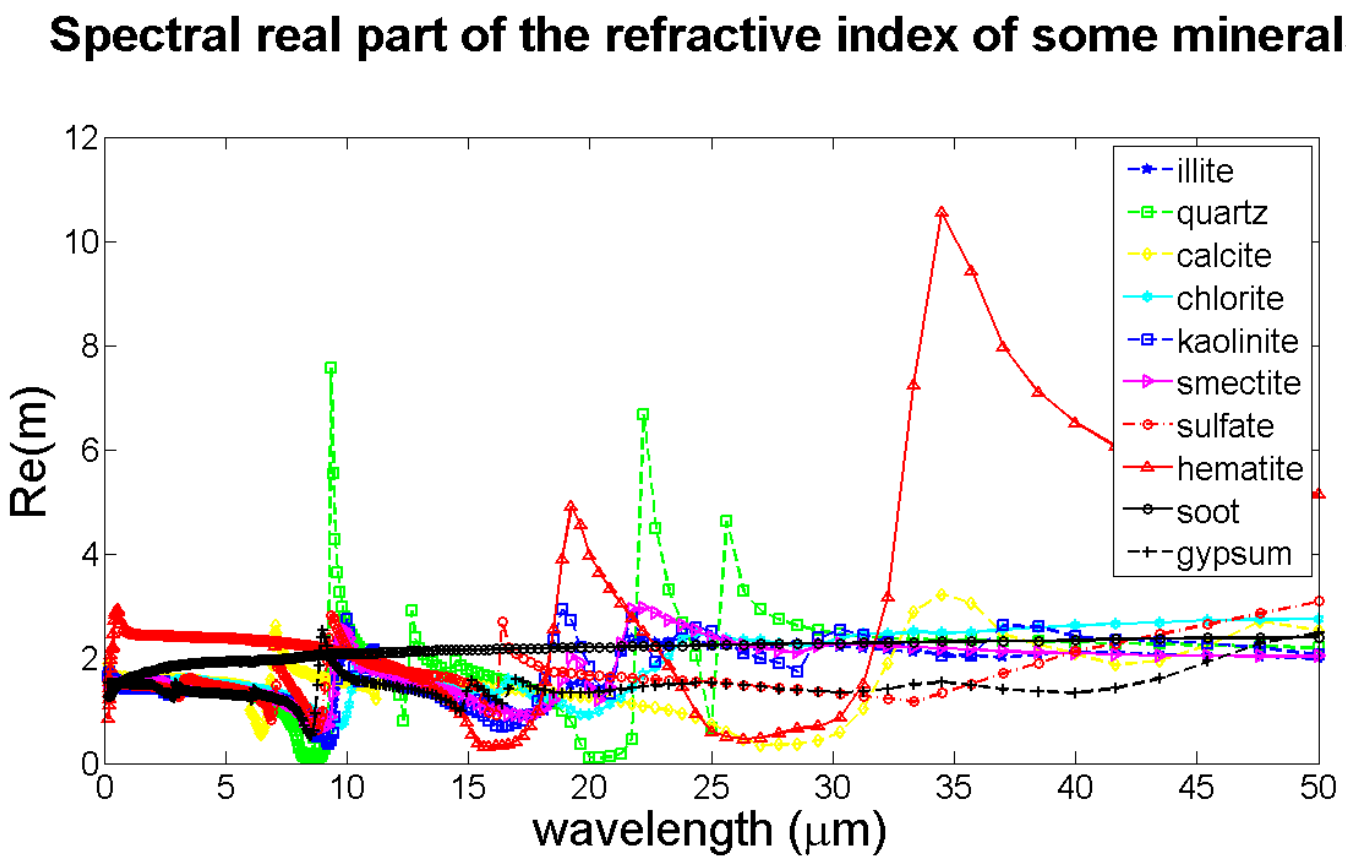

FIG. 3. The real part of refractive indices of different components

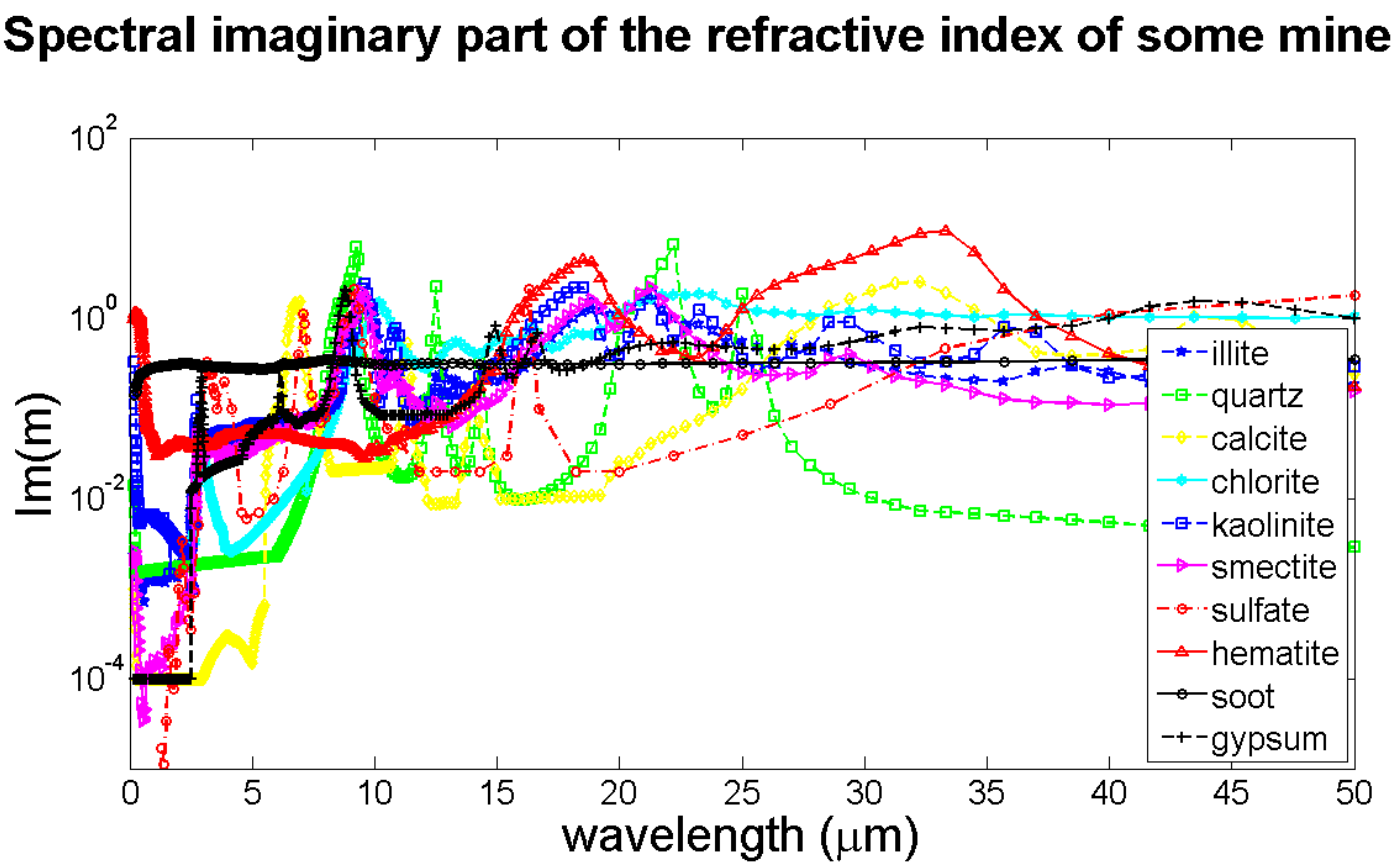

FIG. 4. The imaginary part of refractive indices of different components

3.3 The effective refractive indices

Mineral dust is considered as an aggregate and the Bruggeman effective medium approximation is used to derive the effective refractive indices. Although the calculations using the Maxwell Garnett approximation can give very similar effective refractive indices to those using the Bruggeman approximation (Longtin et al. 1988), we chose the latter because its assumptions seemed to be more adequate for the modeling of multi-component mixtures.

Using the equations in Section 2, the spectral effective refractive indices under the composition models for the Saharan and Asian dust were derived from UV to thermal IR regions. Figure 5 compares the real parts of the effective complex refractive indices for the Saharan dust and Asian dust, and both proved to be very dependent on wavelength. Our values of the real parts are much larger than those of the dust-like data compiled by Levoni et al. (1997) which were widely used by researchers.

Figure 6 shows the imaginary parts of the effective complex indices for Saharan and Asian dust. Again, our values are much larger than those of dust-like data from Levoni et al. (1997). Furthermore, both the real and imaginary refractive indices of Asian dust are much higher than those of Saharan dust, which maybe a result of the large amount of absorptive components added to the Asian composition model.

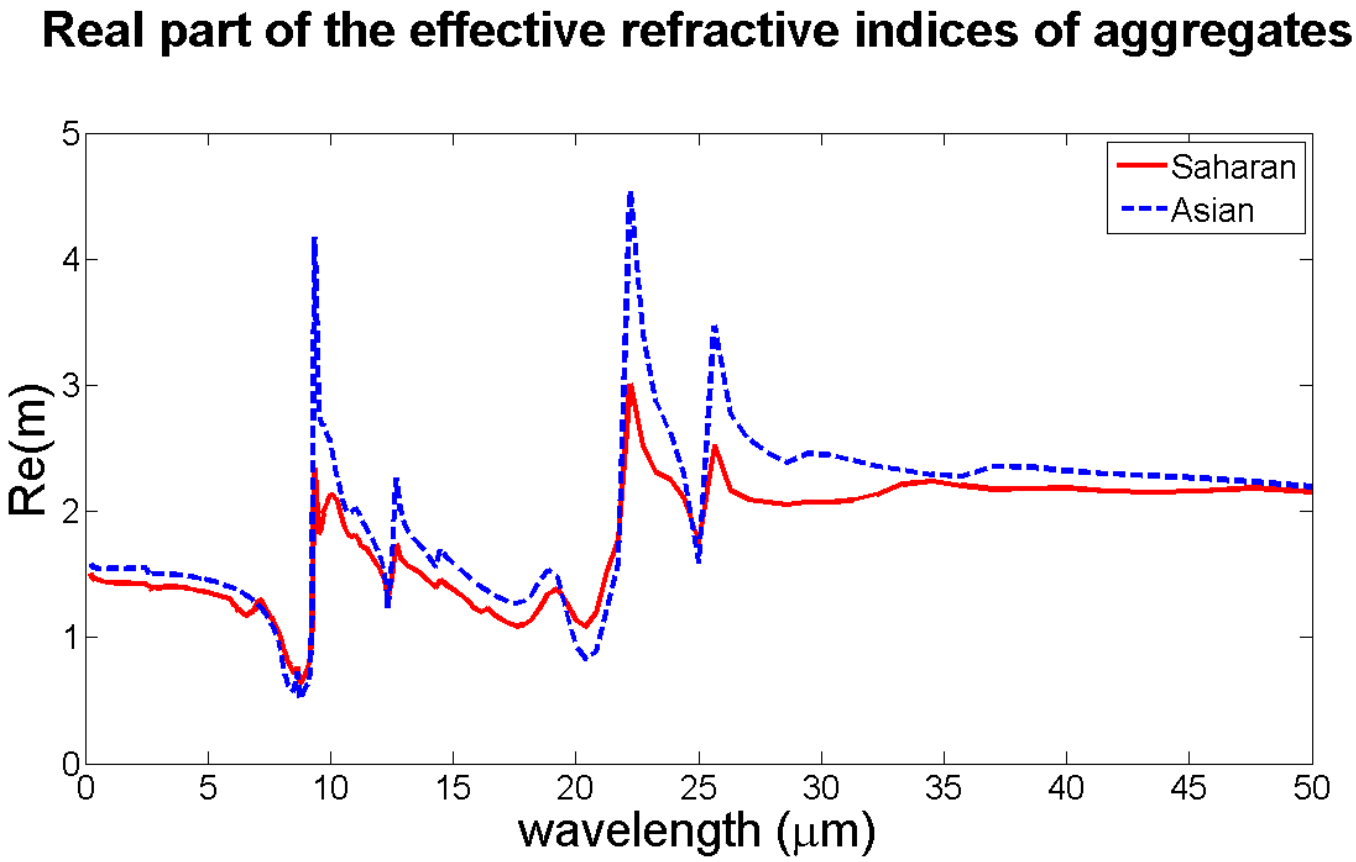

FIG. 5. The real part of the effective complex refractive indices of the Saharan dust and Asian dust

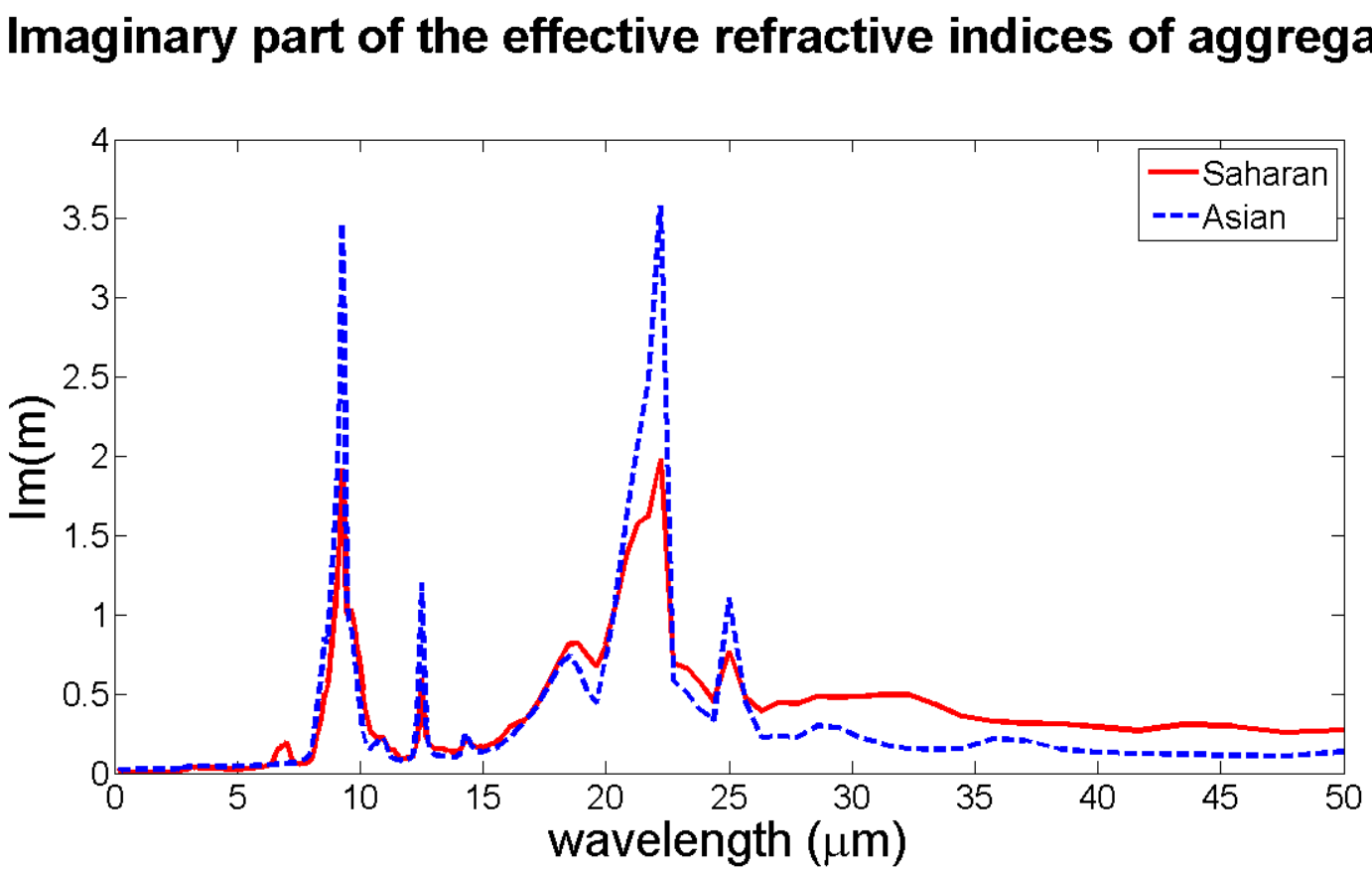

FIG. 6. The imaginary part of the effective complex refractive indices of the Saharan dust and Asian dust

4. OPTICAL PROPERTIES

Analyses of in situ measurements made by Scanning Electron Microscopic and Transmission Electron Microscopy reveal that realistic mineral dust is exclusively composed of irregular shapes (Reid et al. 2003; Jeong 2008; Kandler et al. 2007; Okada et al. 1987; Clarke et al. 2004; Quinn et al. 2004). For simplification in the radiative transfer simulations and remote sensing, the dust particles are often assumed to be homogeneous spheres. However, without considering the nonspherical effect, the dust radiative forcing can be substantially underestimated or overestimated, and incorrect results can be obtained in retrieving dust properties (Dubovik et al. 2002, 2006). Therefore, the mineral dust shapes studied here are assumed to be spheroids. A combination of the T-matrix method (Mishchenko et al. 1997; Waterman 1965) and an improved geometric optics method (IGOM) (Bi et al. 2009; Yang and Liou 1996; Yang et al. 2007) were used to calculate the single-scattering optical properties of the Saharan and Asian dusts from the Rayleigh regime to the geometric optics regime. A database of the optical properties of randomly oriented spheroids has been developed.

4.1 Geometry of the dust particle model

The geometry of the spheroidal model used is shown in Figure 7, where *a* and *b* are two equal semi-radii, and *c* is the polar radius. The aspect ratio ε (different from relative permittivity) of a spheroid is defined as the ratio of the semi-radius and the polar radius, ($\varepsilon_{a/c}$=a/c & $\varepsilon_{\mathrm{b/c}}$=b/c). The size parameter $x = \frac{2\pi c}{\lambda}$ is determined by the semi-

major axis *c*. For spheroids, the two aspect ratios are equal, i.e., $\varepsilon_{a/c} = \varepsilon_{b/c}$. When the aspect ratio is larger than unity it is an oblate spheroid, and when the aspect ratio is smaller than unity it is called a prolate spheroid. For Asian mineral dust, in-situ measurements find the mean aspect ratio is about approximately 1.4. For Saharan dust, the median aspect ratio is approximately 1.6 for particles larger than 500 nm, and it decreases to 1.3 for smaller particles (Kandler et al. 2008). To simplify the computation, the aspect ratios for the Saharan dust and Asian dust were both set at 1.6.

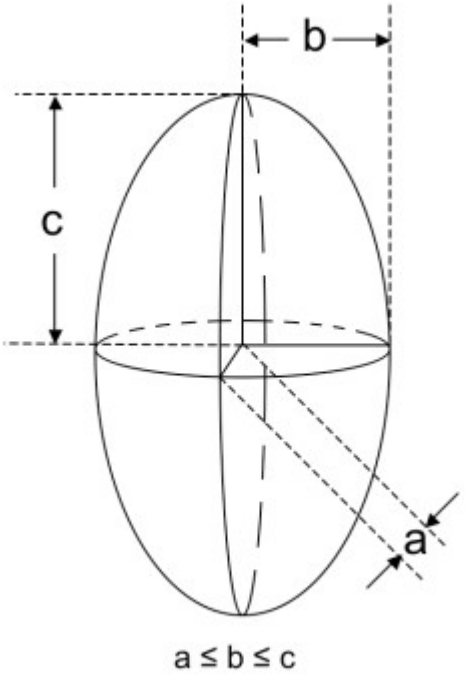

FIG. 7. The geometry of a spheroidal particle model (Meng 2010)

4.2 Single-scattering optical properties

The spectral optical properties of dust which are needed in the radiative transfer simulations include the extinction coefficient Q_e (equal to the scattering and absorption coefficients), the single-scattering albdo ω, and the asymmetry parameter g. These properties, together with the phase matrix are used in the calculation of radiative forcing.

The T-matrix method developed by Mishchenko et al. (1997) and Waterman (1965) provides a powerful approach for computing the scattering properties of nonspherical particles, specifically axially symmetric particles. The method considers the random orientation condition into the scattering properties of nonspherical particles (Yang et al. 2007). For very large particles, an improved geometric optics method (IGOM) (Bi et al. 2009; Yang and Liou 1996; Yang et al. 2007) must be used. The IGOM provides a very good approximation which can be applied to an arbitrary geometry.

For both the T-matrix method and IGOM, the equal-surface-area-sphere radius was used to represent the effective particle size. The size parameter is defined as $x=\frac{2\pi r}{\lambda}$. The T-matrix method was used for size parameters of x<40, and IGOM was used for size parameters of x> 40. Foot (1988) defined the widely used effective particle radius of a spheroid as

$$r_{eff} = \frac{3}{4}\frac{V}{A} \tag{4.1}$$

where A is the projected area of the spheroid and V is the volume

$$V = \frac{4}{3}\pi ab^2 \tag{4.2}$$

and the projected area is A=$\frac{1}{4}S$. Beyer (1981) defined the surface area of a spheroid by

$$S = \begin{Bmatrix} 2\pi b^2 + \pi \frac{a^2}{\varepsilon} \ln \frac{1+\varepsilon}{1-\varepsilon} \\ 2\pi b^2 + \pi \frac{ab}{\varepsilon} \sin^{-1} \varepsilon \end{Bmatrix} \tag{4.3}$$

where the first expression is for oblate spheroids, the second expression is for prolate spheroids, and ε is the eccentricity of the spheroid.

4.3 Bulk scattering properties

The particle size distribution (PSD) used in this study was the modified logarithmic-normal distribution (Shao and Dong 2006):

$$N(D) = \frac{dN}{d\log_{10} d} = \sum_j^J \frac{w_j}{\sqrt{2\pi}\sigma_j} \exp(-\frac{1}{2}(\frac{\ln d - \ln D_j}{\sigma_j})^2) \tag{4.4}$$

where *J* is the number of modes, w_j is the weight for the *jth* mode of the particle-size distribution, D_j is the mode diameter (μm) and σ_j is the standard deviation. These parameters for Saharan dust and Asian dust are from Kandler et al. (2008) and Park and Lee (2004).

Table 3 shows the parameters of the modified lognormal size distributions fitting the measured Saharan dust and Asian dust size distributions.

TABLE 3. Parameters of modified log-normal distributions fitting the measured Saharan dust and Asian dust size distributions.

		J=1	J=2	J=3	J=4
Saharan dust	w_j	0.8424	0.1226	0.0350	3.44×10^{-6}
	D_j	0.08542	0.03529	0.7342	31.08
	σ_j	1.898	5.208	1.749	2.486
Asian dust	w_j	0.0329	0.9671		
	D_j	4.3733	5.7689		
	σ_j	*0.8590*	0.2526		

The effective particle radius r_{eff} is defined as:

$$r_{eff} = \frac{3}{4}\frac{\int_{D_{\min}}^{D_{\max}} V(D)N(D)dD}{\int_{D_{\min}}^{D_{\max}} A(D)N(D)dD} \tag{4.5}$$

In this study, the effective size parameter is approximately 30. The bulk scattering properties are derived by the following formulas

$$\bar{Q}_e = \frac{\int_{D_{\min}}^{D_{\max}} \sigma_e(D)A(D)N(D)dD}{\int_{D_{\min}}^{D_{\max}} A(D)N(D)dD} \tag{4.6}$$

$$\bar{Q}_s = \frac{\int_{D_{\min}}^{D_{\max}} \sigma_s(D)A(D)N(D)dD}{\int_{D_{\min}}^{D_{\max}} A(D)N(D)dD} \tag{4.7}$$

$$\bar{\omega} = \frac{\bar{Q}_e}{\bar{Q}_s} \tag{4.8}$$

$$\bar{P}_{11} = \frac{\int_{D_{\min}}^{D_{\max}} P_{11}(D)\sigma_s(D)A(D)N(D)dD}{\int_{D_{\min}}^{D_{\max}} \sigma_s(D)A(D)N(D)dD} \tag{4.9}$$

where $\bar{Q}_e$ is the mean extinction efficiency, $\bar{Q}_s$ is the mean scattering efficiency, $\bar{\omega}$ is the single-scattering albedo, and $\bar{P}_{11}$ is the mean phase function.

Figure 8 shows the phase matrix of a spheroidal model with the aspect ratio a/c=b/c=1.6 for both Saharan dust and Asian dust at a wavelength of 633 nm. The effective size parameter of Saharan dust is approximately 30. The refractive indices chosen were m=1.449+i0.0018 for Saharan dust, and m=1.545+i0.0233 for Asian dust. Because of the strong absorption of Asian dust, the phase matrix is close to the Rayleigh scattering, which is similar to the results of Yang et al. (2007).

Figure 9 shows the bulk optical properties including the extinction efficiency, the single-scattering albedo, and the symmetry factor. The optical properties are strongly dependent on the spectrum from 0.2 to 25 μm. The optical properties for Saharan dust and Asian dust have a relatively large difference because of the different composition models discussed previously.

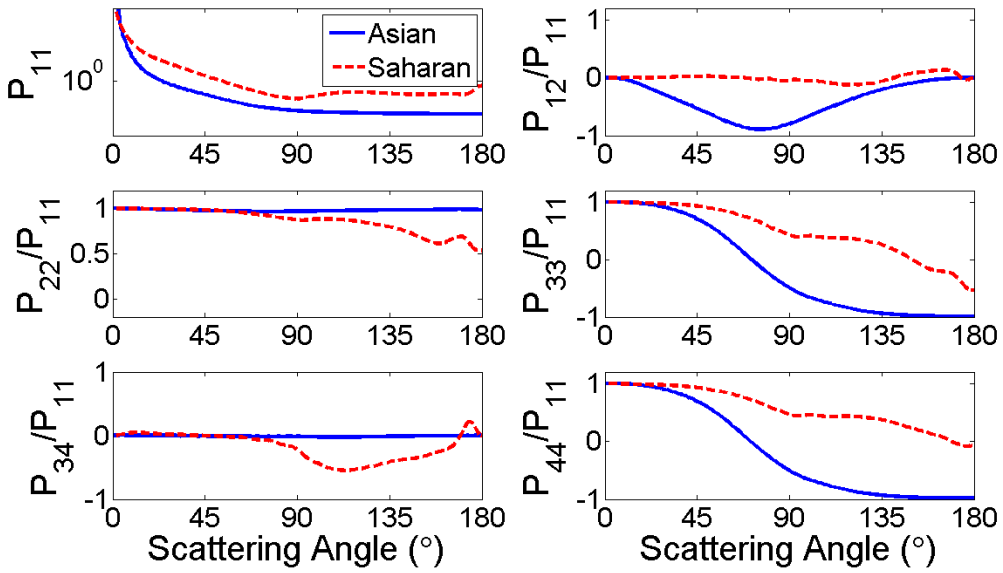

FIG. 8. Bulk phase matrix at a wavelength of 633 nm

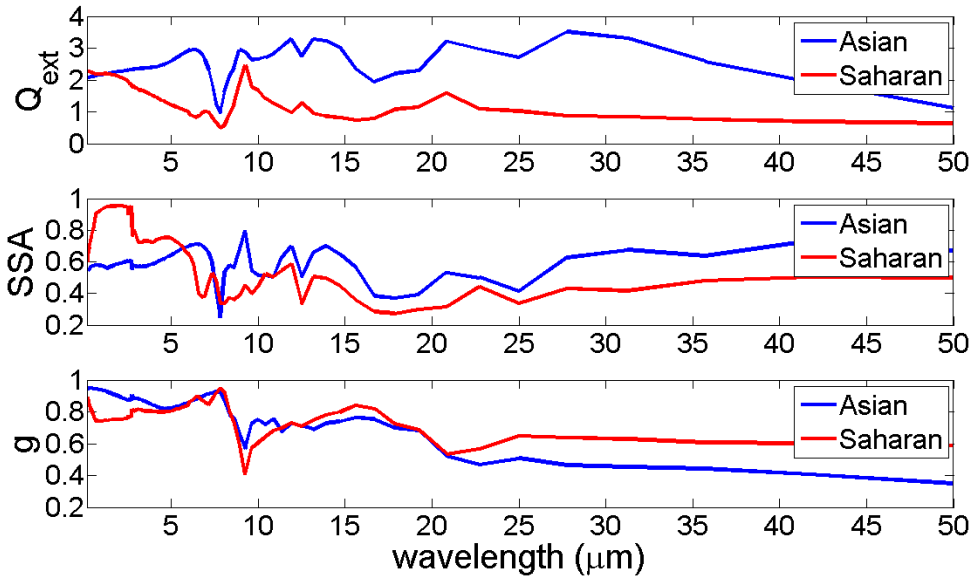

FIG. 9. Bulk optical properties: the extinction coefficient (Q_{ext}), the single-scattering albedo (SSA), and the asymmetry factor (g).

5. RADIATIVE TRANSFER APPLICATION

The optical properties of extinction efficiency, single-scattering albedo, asymmetry factor and phase function computed in the previous sections were applied to radiative transfer simulations. A Rapid Radiative Transfer Model (RRTM) was used to calculate the mineral dust radiative effect in both longwave (IR) and shortwave (solar) regions. The RRTM is based on the line-by-line radiative transfer model (LBLRTM) (Mlawer et al. 1997a, 1997b).

5.1 RRTM bands

Tables 4 and 5 present the RRTM Bands and Included Species for longwave and shortwave. The tables divide the spectrum from solar to thermal IR into 28 bands. Sixteen bands are in the longwave spectral region, in which the absorption due to water vapor, carbon dioxide, ozone, nitrous oxide and methane is considered. Twelve bands are in the shortwave spectral region, in which water vapor, carbon dioxide, oxygen, methane and ozone contribute to the absorption.

TABLE 4. RRTM bands and included species for longwave (Mlawer et al. 1997a)

BAND NUMBER	WAVENUMBER RANGE (cm^{-1})	SPECIES TREATED IN RRTM	
		1050-96 mb	96-0.01 mb
1	10-250	H_2O	H_2O
2	250-500	H_2O	H_2O
3	500-630	H_2O, CO_2	H_2O, CO_2
4	630-700	H_2O, CO_2	CO_2, O_3
5	700-820	H_2O, $CO_2^{(a)}$	CO_2, $O_3^{(a)}$
6	820-980	$H_2O^{(a)}$, (b)	--$^{(a)}$
7	980-1080	H_2O, $O_3^{(b)}$	O_3
8	1080-1180	$H_2O^{(a)}$, (b)	$O_3^{(b)}$
9	1180-1390	H_2O, CH_4	CH_4
10	1390-1480	H_2O	H_2O
11	1480-1800	H_2O	H_2O
12	1800-2080	H_2O, CO_2	--
13	2080-2250	H_2O, N_2O	--
14	2250-2380	CO_2, N_2O	CO_2
15	2380-2600	CO_2	--
16	2600-3250	H_2O, CH_4	CH_4

TABLE 5. RRTM bands and included species for shortwave (Mlawer et al. 1997b)

BAND NUMBER	WAVENUMBER RANGE (cm^{-1})	SPECIES TREATED IN RRTM	
		1050-96 mb	96-0.01 mb
17	3250-4000	H_2O, CO_2	H_2O, CO_2
18	4000-4650	H_2O, CH_4	CH_4
19	4650-5150	H_2O, CO_2	CO_2
20	5150-6150	H_2O	H_2O
21	6150-7700	H_2O, CO_2	CO_2
22	7700-8050	H_2O, CO_2	O_2
23	8050-12850	H_2O	--
24	12850-16000	H_2O, $O_2^{(c)}$	$O_2^{(c)}$
25	16000-22650	$H_2O^{(c)}$	--$^{(c)}$
26	22650-29000	--	--
27	29000-38000	O_3	O_3
28	38000-50000	O_2, O_3	O_2, O_3

(a) Halocarbons implemented as minor species.

(b) CO_2 **implemented as minor species.**

(c) O_3 **implemented as minor species.**

5.2 Band-averaged bulk scattering properties

For RRTM solar bands (wavenumber $\tilde{\upsilon}$>3250cm^{-1} / wavelength λ<3.08μm), the bulk scattering properties at each wavelength should be weighted by the solar irradiance $S(\lambda)$. For RRTM infrared bands (wavenumber $\tilde{\upsilon}$<3250cm^{-1} / wavelength λ>3.08μm), the solar irradiance $S(\lambda)$ is replaced by the Planck function $B(\lambda)$ to represent the thermal infrared emission from a layer (about 1-3 km above the ground surface) of mineral dust at 270.35K. Figures 10 and 11 show the solar irradiance and the Planck function along with the wavelength.

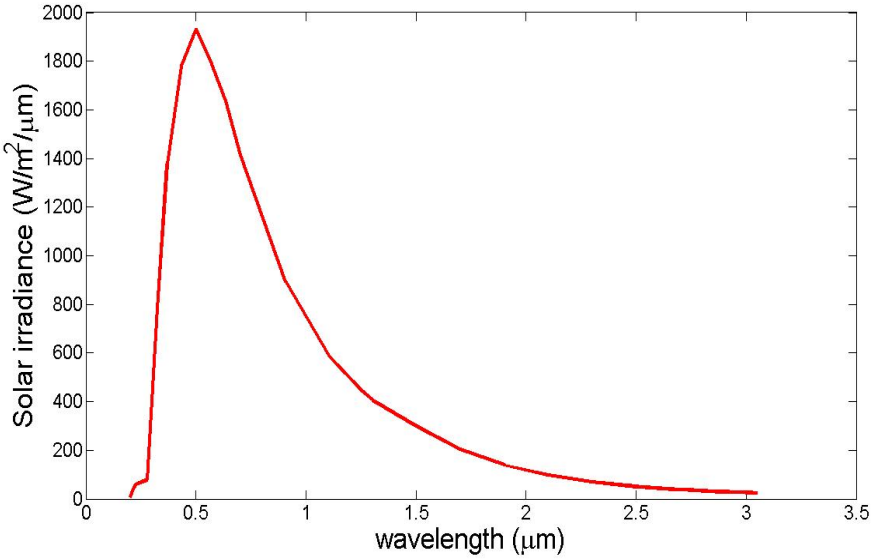

FIG. 10. Solar irradiance from 0.2 to 3 μm

(solar region of the broad band)

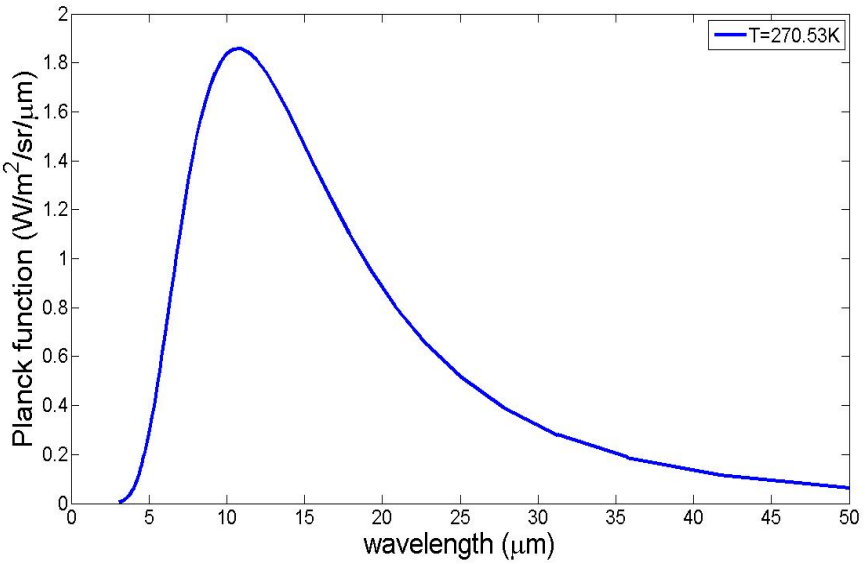

FIG. 11. Planck function from 3 to 50 μm (IR regions of the broad band)

The band-weighted mean scattering properties for shortwave are given by the following expressions:

$$\left\langle Q_{\text{ext}} \right\rangle = \frac{\int_{\lambda_1}^{\lambda_2} \int_{D_{\min}}^{D_{\max}} \left[\sigma_{ext}(\lambda, D)\right] n(D) S(\lambda) dD d\lambda}{\int_{\lambda_1}^{\lambda_2} \int_{D_{\min}}^{D_{\max}} \left[A_i(D)\right] n(D) S(\lambda) dD d\lambda} \tag{5.1}$$

$$\left\langle Q_{\text{sca}} \right\rangle = \frac{\int_{\lambda_1}^{\lambda_2} \int_{D_{\min}}^{D_{\max}} \left[\sigma_{sca}(\lambda, D)\right] n(D) S(\lambda) dD d\lambda}{\int_{\lambda_1}^{\lambda_2} \int_{D_{\min}}^{D_{\max}} \left[A_i(D)\right] n(D) S(\lambda) dD d\lambda} \tag{5.2}$$

$$\left\langle \omega \right\rangle = \frac{\left\langle Q_{\text{sca}} \right\rangle}{\left\langle Q_{\text{ext}} \right\rangle} \tag{5.3}$$

$$\left\langle P_{11}(\theta) \right\rangle = \frac{\int_{\lambda_1}^{\lambda_2} \int_{D_{\min}}^{D_{\max}} \left[P_{11}(\theta, D, \lambda) \sigma_{\text{sca}}(D, \lambda)\right] n(D) S(\lambda) dD d\lambda}{\int_{\lambda_1}^{\lambda_2} \int_{D_{\min}}^{D_{\max}} \left[\sigma_{\text{sca}}(D, \lambda)\right] n(D) S(\lambda) dD d\lambda} \tag{5.4}$$

where *n(D)* is the lognormal particle size distribution used in Section 4, and $\langle\ \rangle$ represents the band-averaging. Within the IR spectrum, the solar irradiance should be replaced by the Planck function.

5.3 Radiative forcing at the TOA and the surface

The flux of clear sky and dust sky were computed independently. We considered the mineral dust layer at the height of approximately 3 km and with a physical depth of approximately 500 m. The solar zenith angle was set at $60°$, the surface albedo was set to be 0.3, and the IR albedo was set to be 0.1. The standard U.S. atmospheric profile was used for the simulation. The dust radiative forcings are shown separately at the TOA and the surface.

Figures 12 and 13 show the shortwave (solar) and longwave (IR) radiative forcing at the top of the atmosphere (TOA) as a function of the optical thickness for mineral dust. The IR dust forcing is always positive, due to the greenhouse heating effect of mineral dust; the solar dust forcing is also positive, meaning the heating effect produced by the dust is more pronounced than the albedo effect. Both the IR and solar dust forcings at the TOA are sensitive to the optical thickness. Comparisons of Asian and Saharan dust forcing find almost no difference in the IR regions; but the solar dust forcing of Asian dust is much higher than that of Saharan dust. The unrealistic amount of absorbing soot in the Asian dust model is responsible for the difference.

Figures 14 and 15 illustrate the solar and IR radiative forcings of mineral dust at the surface. For the IR dust forcing, the inserted dust layer produces small effects at the

surface, due to the strong atmospheric absorption between the surface and the dust layer in the infrared wavelengths. However, the solar dust forcing at the surface is always negative, showing the cooling of the system by the dust albedo effect. Similarly, the IR dust forcing at the surface in Asia is almost no different from that in Sahara; while in the solar wavelengths, a small difference is found.

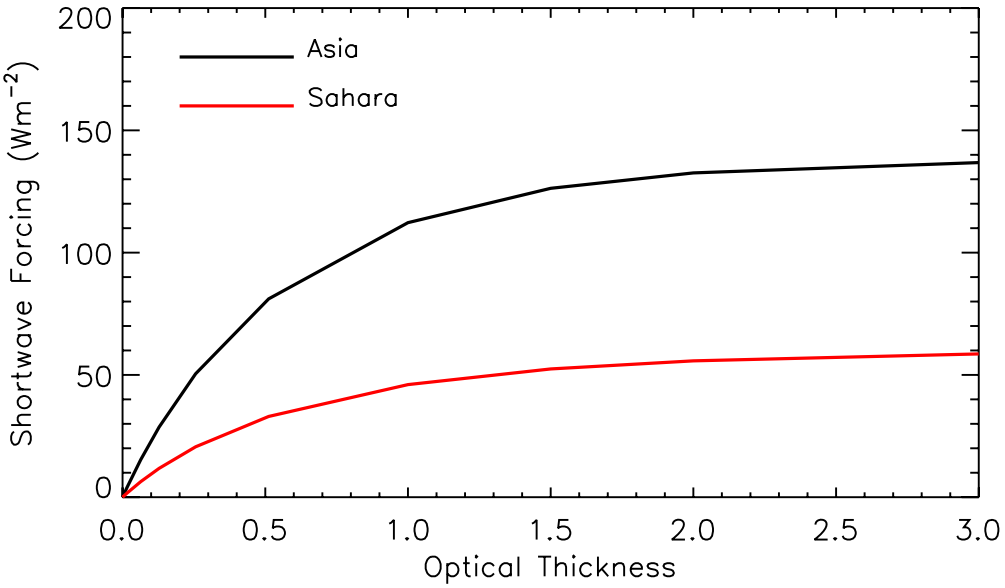

FIG. 12. SW dust radiative forcing at the top of the atmosphere

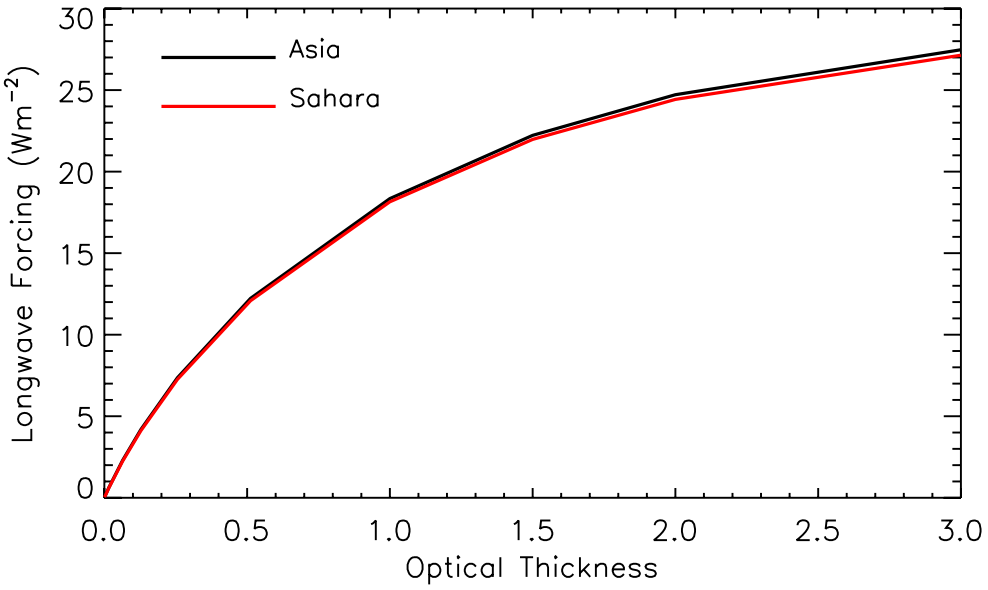

FIG. 13. LW dust radiative forcing at the top of the atmosphere

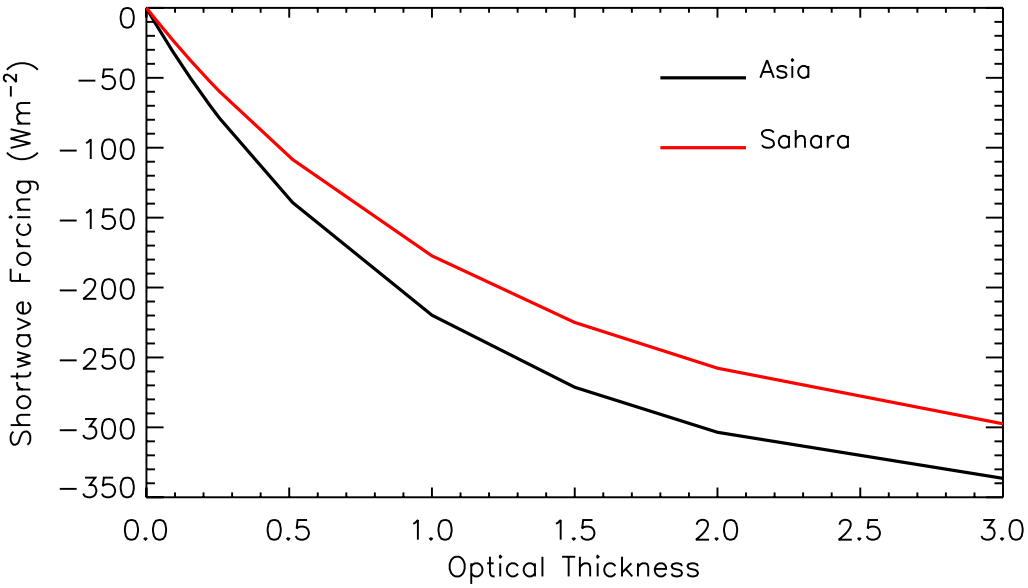

FIG. 14. SW dust radiative forcing at the surface

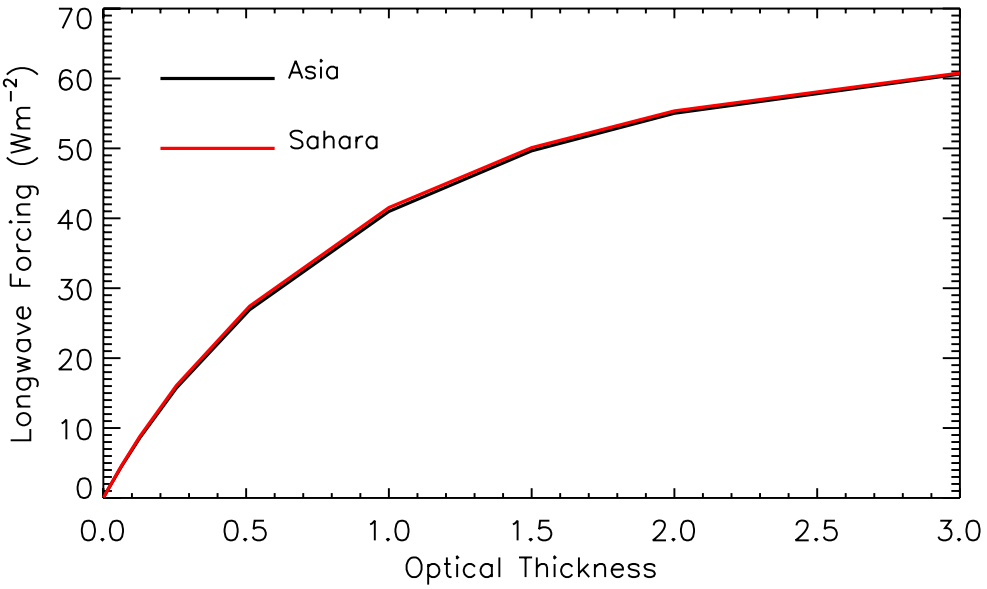

FIG. 15. LW dust radiative forcing at the surface

6. SUMMARY

We have investigated the optical properties of Saharan and Asian dust and applied them to the radiative transfer simulations. The mineralogical composition models for Saharan and Asian dust were assumed from the in-situ measurements. Effective refractive indices of Saharan dust and Asian dust were derived by compiling a data set from reported observations in the literature. Ten components were considered in Saharan dust, and eight components in Asian dust; however, the averaged approximation requires validation by more study. The effective complex refractive indices of Saharan and Asian dust were derived by the Bruggeman effective medium approximation.

A combination of the T-matrix method and an improved geometric optics method (IGOM) were used to calculate the single-scattering optical properties of the Saharan dust and Asian dust from the Rayleigh regime to the geometric optics regime. The optical properties are strongly dependent on the chemical compositions of Saharan and Asian dust.

A Rapid Radiative Transfer Model (RRTM) was applied to compute the radiative forcings of dust at both the TOA and the surface. At the TOA, the heating effect of IR and solar dust forcing is pronounced. At the surface, IR dust forcing shows a heating effect, but the solar dust forcing illustrates a cooling effect. In the IR region, dust forcing is not sensitive to the composition of the mineral dust.

REFERENCES

Arakawa, E. T., P. S. Tuminello, B. N. Khara, M. E. Millham, S. Authier, J. Pierce, 1997: Measurement of optical propertied of small particles. *1997 Scientific Conference on Obscuration and Aerosol Research Aberdeen Proving Ground, Maryland*.

Batten, C. E., 1984: Spectral optical constants of soots from polarized angular reflectance measurements. *App. Opt.*, **24,** 1193-1199.

Bedidi, A., and B. Cervelle, 1993: Light scattering by spherical particles with hematite and goethitelike optical properties: effect of water impregnation. *J. Geophys, Res.*, **98**, 11941-11952.

Beyer, W. H., 1981: CRC standard mathematical tables (26th ed.). Boca Ration, FL: CRC Press, 120.

Bi, L., P. Yang, G. W. Kattawar, and R. Kahn, 2009: Single-scattering properties of trianxial ellipsoidal particles for a size parameter range from Rayleigh to geometric regimes, *App. Opt.*, **48**, 114-126.

Bohren, C. F., and D. R. Huffman, 1983: *Absorption and Scattering of Light by Small Particles*. New York: Wiley-Interscience, 530pp.

Bruggeman, D. A. G., 1935: Ann. Phys., Lpz., **24**, 636.

Carlson, T., 1979: Atmospheric Turbidity in Saharan Dust Outbreaks as Determined by Analyses of Satellite Brightness Data. *Mon. Wea. Rev.*, **107**, 322-335.

Clarke, A. D., Y. Shinozuka, V. N. Kapustin, et al., 2004: Size distributions and mixtures of dust and black carbon aerosol in Asian outflow: Physsiochemistry and optical properties. *J. Geophys, Res.*, **109**, D15S09.

Dubovik, O., B. N. Hilben, T. Lapyonok, A. Sinyuk, M. I. Mishchenko, et al., 2002: Non-spherical aerosols retrieval method employing light scattering by spheroids. *Geophys. Res. Lett.*, **29,** 10, 1415, 10.1029/2001GL014506.

Dubovik, O., A. Sinyuk, T. Lapyonok, et al., 2006: The applicaition of spheroid models to account for aerosol particle nonsphericity in remote sensing of desert dust. *J. Geophys, Res.-Atmos.*, **1111**, D11208.

Egan, W. G., and T. W. Hilgeman, 1979: *Optical Properties of Inhomogeneous Materials*, Academic, New York, 235pp.

Foot, J. S., 1988: Some observations of the optical properties of clouds, ll , Cirrus. *Q. J. R. Meteorol. Soc.*, **114**, 145-164.

Gillespie, J. B. and J. D., Lindberg, 1992: Ultraviolet and visible imaginary refractive index of strongly absorbing atmospheric particulate matter. *App. Opt.*, **31,** 2112-2115.

Glotch, T. D., G. R. Rossman, and O. Aharonson, 2007: Mid-infrared (5-200 μm) reflectance spectra and optical constants of ten phyllosilicate minerals. *Icarus*, **192**, 605-622.

Haywood, J., P. Francis, S. Osborne, M. Glew, N. Loeb, et al., 2003: Radiative properties and direct radiative effect of Saharan dust measured by the C-130 aircraft during SHADE: 1. Solar spectrum. *J. Geophys, Res.* **108**. D18, 8577, doi: 10. 1029/2002JD002687.

Henning, T., B. Begemann, H. Mutxchke, and J. Dorschner, 1995: Optical properties of oxide dust grains. *Astron. and Astrophys. Suppl. Ser.,* **112**, 143.

Hsu, N., S. Tsay, M. King, and J. Herman, 2004: Aerosol properties over bright-reflecting source regions. *IEEE Trans. Geosci. Remote Sensing,* **42**, 557-569.

Hu, Y., M. Vaughan, Z. Liu, et al., 2007: The depolarization- attenuated backscatter relation: CALIPSO lidar measurements vs. theory. *Opt. Express,* **15**, 5327-5332.

Huebert B. J., T. Bates, P. B. Russell, G. Shi, Y. J. Kim, et al., 2003: An overview of ACE-Asia: Strategies for quantifying the relationships between Asian aerosols and their climatic impacts. *J. Geophys, Res.*, **108**, D23, 8633, doi:10.1029/2003JD003550.

Husar, R., J. Prospero, and L. Stowe, 1997: Characterization of tropospheric aerosols over the oceans with the NOAA advanced very high resolution radiometer optical thickness operational product. *J. Geophys, Res.*, **102**, 16889-16909.

IPCC, Forster P., and coauthors, 2007: Changes in atmospheric constituents and in radiative forcing. *Climate Change 2007: The Physical Science Basis,* S. Solomon, et al., Eds, Cambridge Univerity Press, 131.

Ivlev, L. S., and S. I. Popoca, 1973: The complex refractive indices of substances in the atmospheric aerosol dispersed phase, Izv. *Atmos. Oceanic Phys.*, **9**, 587-591.

Jacob, D. J., J. H. Crwford, M. M. Kleb, V. S. Connors, R. J. Bendura, et al., 2003: Transport and chemical evolution over the Pacific (TRACE-P) aircraft mission: Design, execution, and first results, *J. Geophys, Res.*, **108**, D20, 9000, doi:10.1029/2002JD003276.

Jazembski, M. A., M. L. Norman, K. A. Fuller, V. Srivastava, and D. R. Cutten, 2003: Complex refractive index of ammonium nitrate in the 2-20 μm spectral range. *App. Opt.*, **42**, 922-930.

Jeong, G.Y., 2008: Bulk and single-particle mineralogy of Asian dust and a comparison with its source soils. *J. Geophys, Res.*, **113**, D02208.

Jones, C., N. Mahowald, and C. Luo, 2004: Observational evidence of African desert dust intensification of easterly waves. *Geophys. Res. Lett.*, **31**. Doi: 10.1029/2004GL020107.

Kandler, K., N. Benker, U. Bundke, E. Cuevas, M. Ebert, et al., 2007: Chemical composition and complex refractive index of Saharan Mineral Dust at Izana, Tenerife (Spain) derived by electron microscopy. *Atmos. Env.*, **41**, 8058-8074.

Kandler, K., L. Schutz, C. Deutscher, M. Ebert, H. Hofmann, et al., 2008: Size distribution, mass concentration, chemical and mineralogical composition and derived optical parameters of the boundary layer aerosol at Tinfou, Morocco, during SAMUM 2006. *Tellus*, **61B**, 32-50.

Kaufman, Y., I. Koren, L. Remer, D. Tanre, P. Ginoux, and S. Fan, 2005: Dust transport and deposition observed from the Terra-Moderate Resolution Imaging Spectroradiometer (MODIS) spacecraft over the Atlantic Ocean. *J. Geophys, Res.*, **110**. D10S12. Doi: 10.1029/2003JD004436.

Levoni C, M. Cervino, R. Guzzi and F. Torricella, 1997: Atmospheric aerosol properties: a database of radiative characteristics for different components and classes. *App. Opt.*, **36**, 8031-8041.

Long, L. L., M. R. Querry, R. J. Bell and R. W. Alexander, 1993: Optical properties of calcite and gypsum in crystalline and powdered form in the infrared and far-infrared. *Infrared Phys. Technol.*, **34**, 191-201.

Longtin, E. R., E. P . Shettle, J. R. Hummel, and J. D. Pryce, 1988: *A wind dependent desert aerosol dust model: Radiative properties*. Air Force Geophys. Lab., Air Force Syst. Command, Hanscom Air Force Base, Mass, AFGL-TR-88-0112, 105 pp.

Lucarini V., J. J. Saarinen, K.-E. Peiponen, and E. M. Vartiainen, 2005: *Kramers-Kronig Relations in Optical Materials Research*. Heidelberg: Springer. ISBN 3-540-23673-2, 157pp.

Marra, A. C., A. Blanco, S. Fonti, A. Jurewicz and V. Orofino, 2005: Fine hematite particles of Martian interest: absorption spectra and optical constants. *J. Phys.: Conf. Ser.*. **6,** doi:10.1088/1742-6596/6/1/013.

Maxwell Garnett, J. C., 1904: Colours in metal glasses and in the metallic films. Philos. Trans. *R. Soc.*, **203**, 385-420.

McConnell, C. L., E. J. Highwood, H. Coe, P. Formenti, B. Anderson, S. Osborne, et al., 2008: Seasonal variations of the physical and optical characteristics of Saharan dust: Results form the Dust Outflow and Deposition to the Ocean (DODO) experiment. *J. Geophys, Res.*, **113**, doi:10.1029/2007JD009606.

Meng, Z., 2010: Light scattering problem and its application in atmospheric science. M.S. thesis, Dept. of Atmospheric Science, Texas A&M University, 94pp.

Mishchenko, M. I., L. D. Travis, W. B. Rossow, and R. A. West, 1997: Modeling phase functions for dustlike tropospheric aerosols using a mixture of randomly oriented polydisperse spheroids. *J. Geophys, Res.*, **102**, 16831-16847.

Mlawer, E. J., S. J. Taubman, P. D. Brown, M. J. Iacono, and S. A. Clough, 1997a: Radiative transfer for inhomogeneous atmospheres: RRTM, a validated correlated-k model for the longwave. *J. Geophys. Res.*, **102**, 16663-16682.

Mlawer, E. J., and S. A. Clough, 1997b: *On the extension of rapid radiative transfer model to the shortwave region,* Proceedings of the 6th Atmospheric Radiation Measurement (ARM) Science Team Meating, U. S. Department of Energy, 223-226.

Mooney, T., and R. F. Knacke, 1995: Optical constants of chlorite and serpentine between 2.5 and 50 microns. *Icarus*, **64**, 493-502.

Okada, K., A. Kobayashi, Y. Iwasaka, H. Naruse, T. Kanaka, and O. Nemoto, 1987: Features of individual Asian dust-storm particles collected at Nagoya. *J. M. S. J.*, **65**, 515-521.

Osborne, S., B. Johnson, J. Haywood, and C. McConnell, 2008: Physical and optical properties of mineral dust aerosol during the North Atlantic Oscillation. *Nat.*, **387**, 691-694.

Otto, S., E. Bierwith, B. Weinzierl, K. Kandler, M. Esselborn, et al., 2009: Solar radiative effects of a Saharan dust plume observed during SAMUM assuming speroidal model particles. *Tellus B,* **61B**, 270-296.

Park, S. and E. Lee, 2004: Parameterization of Asian dust (Hwangsa) particle-size distributions for use in dust emission models. *Atmos. Env.*, **38**, 2155-2162.

Palmer, K. F. and D. Williams, 1975: Optical constants of sulfuric acid: application to the clouds of Venus. *App. Opt.*, **14,** 208-219.

Petzold A., K. Rasp, B. Weinzierl, M. Esselborn, T. Hamburger, et al., 2008: Saharan dust absorption and refractive index from aircraft-based observations during SAMUM 2006. *Tellus,* **61**, 118-130.

Peterson, J. T., and J. A. Weinman, 1969: Optical properties of quartz dust particles in infrared wavelength. *J. Geophys, Res.*, **28**, 6947-6952.

Philipp, H. R., 1985: *Handbook of Optical Constants of Solids*. Academic Press, Inc. 719-747.

Prospero, J., P. Ginoux, O. Torres, S. Nicholson, and T. Gill, 2002: Environmental characterization of global sources of atmospheric soil dust identified with the NMBUS 7 Total Ozone Mapping Spectrometer (TOMS) absorbing aerosol product. *Rev. of Geophys.*, **40**, doi: 10.1029/200RG00095.

Popova, S. I., T. S. Tolstkh and V. T. Vorobev, 1972: Optical characteristics of amorphous quartz in the 1400-200/cm region. *Opt. Spectrosc.*, **33**, 444-445.

Quinn, P. K., D. J. Coffman, T. S. Bates, E. J. Welton, D. S. Covert, et al., 2004: Aerosol optical properties measured on board the Ronald H. Brown during ACE-Asia as a function of aerosol chemical composition and source region. *J. Geophs. Res.*, **109**, doi: 10.1029/2003JD004010.

Querry, M. R., G. Osboren, K. Lies, R. Jordon, and R. M. Coveney,. 1978: Complex refractive index of limestone in the visible and infrared. *App. Opt.*, **17**, 353-356.

Querry, M. R., 1985: *Optical constants*, U. S. Army CRDEC, Contractor Report, Aberdeen Proving Ground, Md..

Querry, M. R., 1987: Optical constants of minerals and other materials from the millimeter to the UV, *Rep. CRDEC-CR-88009, U. S. Army, Aberdeen, MD.*

Reid, E. A., J. S. Reid, M. M. Meier, M. R. Dunlap, S. S. Cliff, A. Broumas, K. Perry, and H. Maring, 2003: Characterization of African dust transported to Puerto Rico by individual particle and size segregated bulk analysis. *J. Geophs. Res.—Atmospheres*, **108**, doi:10.1029/2002JD002935.

Roush, T., J. Pollack, and J. Orenberg, 1991: Derivation of mid-infrared optical constants of some silicates and palagonite. *Icarus*, **94**, 191-208.

Schmetz, J., P. Pili, S. Tjemkes, D. Just, J. Kerkmann, S. Rota, and A. Tatier, 2002: An introduction to meteosat second Generation (MSG). *Bull. Am. Meteorol. Soc.*, **83**, 977-992.

Shao, Y. and C. H. Dong, 2006: A review on East Asian dust storm climate, modeling and monitoring. *Glo. Pla. Cha.*, **52**, 1-22.

Shettle, E. P. and R. W. Fenn, 1979: Models of the aerosols of the lower atmosphere and the effects of humidity variations on their optical properties. Project 7670, Air Force Geoph. Lab., Massachusetts.

Sokolik, I. N., and O. B. Toon, 1999: Incorporation of mineralogical composition into models of the radiative properties of mineral aerosol from UV to IR wavelengths. *J. Geophs. Res.*, **104**, 9423-9444.

Steyer, T. R., K. L. Day, and D. R. Huffman, 1974: Infrared absorption by small amorphous quartz sphere. *Appl. Opt.*, **13**, 1586-1590.

Toon, O. B., J. B., Pollack, and C. Sagan, 1977: Physical properties of the particles composing the Martian dust storm of 1971-1972. *Icarus*, **30**, 663-696.

Torres, O., A. Tanskanen, B. Veihelmann, C. Ahn, R. Braak, P. Bhartia, P. Veefkind, and P. Levelt, 2007: Aerosols and surface UV products from Ozone Monitoring Instrument observations: an overview. *J. Geophs. Res.*, **112**, D24S47, doi:10.1029/2007JD008809.

Tropf, W., 1998: *Handbook of Optical Constants of Solids*. San Diego, CA: Elsevier Academic, 653-682.

Volz, F. E., 1973: Infrared optical constants of ammonium sulfate, Sahara dust, volcanic pumice, and flyash. *App. Opt.*, **12**, 564-568.

Waterman, P. C., 1965: Matrics formulation of Electromagnetic scattering. *Proceedings of the IEEE,* **53**, 805-812.

WCRP, World Climate Research Program, 1986: A preliminary cloudless standard atmosphere for radiation computation. WCP-112, WMO/TD-NO. **24**, 53pp.

Yang, P., and K. N. Liou, 1996: Geometric-optic-integral-equation method for light scattering by nonspherical ice crystals. *App. Opt.,* **35**, 6568-6584.

Yang, P., Q. Feng, G. Hong, G. W. Kattawar, W. J. Wiscombe, M. Mishchemko, et al., 2007: Modeling of the scattering and radiative properties of nonspherical dust-like aerosols. *J. of Aero. Sci*., **38**, 995-1014.

VITA

Name:	Guangyang Fang
Address:	Department of Atmospheric Sciences, MS 3150, Texas A&M University, College Station, Texas 77843-3150 US
Email Address:	fang.gy@tamu.edu
Education:	B.S., Atmospheric Sciences, Nanjing University of Information Science & Technology, 2006 M.S., Atmospheric Electricity, Chinese Academy of Sciences, 2010 M.S., Atmospheric Sciences, Texas A&M University, 2012